Energy spectra of the first TGE observed on Zugspitze by the SEVAN light detector compared with the energetic TGE observed on Aragats

A. Chilingarian [a,*], T. Karapetyan [a], B. Sargsyan [a], J. Knapp [b], M. Walter [b], T. Rehm [c]

[a] *Alikhanyan National Lab (Yerevan Physics Institute), Yerevan 0036, Armenia*
[b] *Deutsches Elektronen-Synchrotron DESY, Hamburg, Germany*
[c] *Environmental Research Station Schneefernerhaus (UFS), Germany*

ARTICLE INFO

ABSTRACT

The energy spectra of Thunderstorm ground enhancement (TGE) electrons and gamma rays are the key evidence for proving the origin of enhanced particle fluxes from thunderclouds. Till now, the electron energy spectrum was measured only by the Aragats large scintillation spectrometer ASNT. We changed the electronics board of the SEVAN detector installed at the Umwelt-Forschungs-Station (UFS, Schneefernerhaus, 2650 m asl) to allow these vital measurements near the top of the Zugspitze. The new electronics of the SEVAN detector, supplied with logarithmic ADC, for the energy release measurements up to 50 MeV (the thickness of the spectrometric scintillator is 25 cm). Thus, by measuring energy releases well above 3 MeV, we unambiguously separate Radon progeny gamma radiation from the electrons and gamma-ray relativistic runaway avalanches. Using the different energy release histograms allows for separating charged and neutral particles, enabling the disentangling of electron and gamma-ray energy spectra. On May 23, 2023, the first TGE was registered on Zugspitze by the SEVAN detector. The gamma-ray flux enhancement was 44%, corresponding to the observed count rate peak enhancement of 44σ. The gamma-ray energy spectrum was recovered, maximum energy is 60 MeV. On the same day, a large TGE was observed on Aragats. The TGE maximum flux overpasses the fair-weather flux by 207%, equivalent to a 1-minute peak significance of 400σ. Maximum energy of electrons is 50 MeV, gamma rays – 45 MeV. In this context, we will explore and explain the new capabilities of the SEVAN detector installed on Zugspitze and the rearranged similar detector on Aragats. We also present and compare electron and gamma-ray energy spectra from Aragats TGE and gamma-ray energy spectrum from Zugspitze.

1. Introduction

SEVAN (Space Environment Viewing and Analysis Network) is a network of particle detectors located at middle to low latitudes, primarily on mountain peaks [1]. It started as a project of the International Heliophysical Year (IHY-2007) and is currently operational as part of the International Space Weather Initiative (ISWI). For almost 15 years, the SEVAN detectors have measured the time series of charged and neutral particle count rates. These particles are produced in cascades originating in the atmosphere from nuclear interactions of galactic and solar protons and nuclei (GCR and SCR).

Three SEVAN detectors are operating in Armenia (on the slopes of Mt. Aragats: 40.25N, 44.15E, altitudes 1600, 2000, 3200 m), in Croatia (Zagreb observatory: 45.82N, 15.97E, altitude 120 m), in Bulgaria (Mt. Musala: 42.1N, 23.35E, altitude 2930 m), in Slovakia (Mt. Lomnicky

Stit: 49.2N, 20.22E, altitude 2634 m, on Mileshovka hill (50.6N, 13.9E, altitude 837 m) in Czech republic, in Germany at Zugspitze Schneefernerhaus (47.42N, 10.98E, altitude 2650 m), and DESY Hamburg (53.5730N, 9.8810E, altitude 20m).

The primary goal of the SEVAN network was the basic research of solar physics, solar-terrestrial connections, and space weather [2], as well as establishing services for alerting and forecasting dangerous consequences of space storms [3]. The significant advantage of SEVAN detectors is they measurement of solar modulation effects simultaneously in fluxes of low-energy electrons and gamma rays, neutrons, and high-energy muons [4]. The highest energy SCR comprising the so-called solar energetic particle (SEP) event generates particle showers that can reach surface particle detectors, initiating ground-level enhancement (GLE). However, following the largest GLE of January 2005, the Sun entered a calm epoch, and the solar activity cycles of 24

and 25 did not produce any significant SEP events to test the capabilities of the SEVAN network.

As a result, the SEVAN network was employed to investigate particle bursts connected to the Extensive Air Shower (EAS) phenomenon and atmospheric processes, known as high-energy physics in the atmosphere (HEPA) [5]. Studies on thunderstorm ground enhancements (TGEs) [6, 7], terrestrial gamma-ray flashes (TGFs) [8], and gamma-ray glow [9–11] have shed light on the complex interactions between the atmosphere and cosmic ray fluxes. It is widely accepted that all three processes result from electron acceleration in atmospheric electric fields. Free electrons from small and large EASs [12] gain more energy than they lose through ionization when they enter strong enough electric fields. These accelerated electrons knock out atomic electrons, creating bremsstrahlung gamma rays, and so on. Initially known as runaway breakdown (RB, [13]), this process is now referred to as relativistic runaway electron avalanche (RREA, [14–16]) and continues until the electric field strength is sufficient enough to sustain the electron-gamma ray avalanche. RREA is responsible for the large-scale multiplication of particles that are observed on Earth's surface (TGE), in space (TGF), or those found in the atmosphere by particle detectors on balloons and aircraft (gamma glow). RREA is a "threshold" process controlled by the electric field's strength and air density [17]. The atmospheric electric field also generates modification of the electron energy spectra (MOS, [18,19]), which operates on a smaller scale but is not limited to a specific electric field. To understand HEPA phenomena, particle detectors and spectrometers must detect elementary particles within the energy range of 0.3-100 MeV. Field meters, meteorological sensors, and all-sky cameras should accompany particle detection. The analysis of multivariate information resulted in models of how electrons, positrons, muons, neutrons, and photons interact with atmospheric electric fields and air. Physicists from the Yerevan Physics Institute and their colleagues from the European SEVAN network conducted the first-ever TGE searching campaign using SEVAN detectors at the highest peaks in Eastern Europe and Germany [20]. The TGE detection campaign operates 24/7 at Aragats, Lomnicky Stit, Musala, and Zugspitze mountains. Despite the large variety of intensity, duration, and shapes of detected TGEs, they share many common characteristics. Usually, the largest TGEs last only a few minutes, during which particle fluxes can increase to tens or even hundreds of times the fair-weather values. Lightning flashes often abruptly terminate them, and during TGEs, lightning activity is usually suppressed [21,22]. Recently published TGE catalogs comprise 318 TGE events recorded on Aragats [23] and 80 air glow observed on the western seashore of Japan [24], providing evidence that RREA is a universal mechanism operating in thunderous atmospheres across the globe.

Solar and atmospheric physics are interconnected fields that rely on exchanging results to explain particle bursts and understand the influence of solar flares, explosions in the galaxy and beyond, as well as the impact of atmospheric electric fields on the changing fluxes of secondary cosmic rays that reach the Earth's surface. Given the rapidly rising natural disasters, geophysical research is becoming increasingly important in the coming decades.

2. Instrumentation

In April 2023, the SEVAN detector relocated from DESY Zeuthen to the Umwelt-Forschungs-Station Schneefernerhaus (UFS, 2650 m a.s.l.), where Joachim Kuettner discovered a tripole structure of the electric field in brilliant experiments performed in 1945-1949 [25]. There is an ongoing cosmic ray research program at UFS, including measuring the energy spectra of atmospheric neutrons with an extended-range Bonner sphere and other detectors [26]. The neutron data has been used to investigate temporal variations in the cosmic radiation intensity and local effects like soil moisture and snow cover. The SEVAN detector was required to be smaller in size and weight to comply with building regulations. As a result, the lower third scintillator setup and lead filters

were removed. However, the newly developed electronics board has added a new capability to the SEVAN detector. It can now measure the energy spectra of charged and neutral particle fluxes. In this way, the SEVAN at Zugspitze becomes an advanced detector for solar and high-energy atmospheric physics research. During TGEs, the upper 5 cm thick scintillator detects a significant increase in TGE particles. By using the veto signal from the upper scintillator, fluxes of TGE electrons and gamma rays can be separated. The coincidence techniques can select direct neutrons from the violent solar bursts and neutrons produced in the Earth's atmosphere by the photonuclear reactions of TGE gamma rays. In this way, we can recover the energy spectrum of neutrons from solar flares and gamma rays and electrons from TGEs. The SEVAN detector, previously measuring only count rates, has been transformed into a powerful spectrometer capable of measuring different species of secondary cosmic rays from galactic and atmospheric accelerators thanks to the modernized DAQ board. The list of available information from modernized SEVAN will be as follows:

- 1-minute count rates of stacked 5 and 25-cm thick scintillators.
- 1-minute count rates of the coincidences "01", signal only in 25 cm scintillator; "10" – signal only in the upper 5-cm thick scintillator, and "11" – signal in both scintillators.
- Histograms of energy releases in both scintillators. Histograms corresponding to the coincidences mentioned above. 1-minute histograms of energy releases stored continuously.

A coincidence of "10" identifies particles that generate a signal in the upper scintillator while bypassing the lower scintillator. Thus, the particle samples and energy release histograms selected by the "10" coincidence will experience an enrichment of charged particles. In contrast, the samples and histograms selected by the "01" coincidence will be enriched by neutral particles. In addition, the "11" coincidence will select high-energy charged particles, specifically muons and TGE electrons.

Table 1 shows the results of the SEVAN light detector response calculation with simulated cosmic ray flux at Zugspitze obtained with the EXPACS WEB calculator [27]. As we can see in Table 1, the "01" coincidence (signal only in the bottom scintillator) comprises 34% of neutrons and 59% of gamma rays. The 25 cm scintillator selects 16% of neutrons and 27% of gamma rays. With the "01" coincidence, we significantly increase the proportion of neutral particles in the sample (purity). An enlarged proportion of neutral particles enables the identification of the TGE gamma rays and the GLE neutrons. Indeed, the "01" coincidence cannot differentiate between neutrons and photons. However, most of the additional neutral particles are gamma rays during the TGE, while they are neutrons during the GLE. Both cases do not intersect and can be easily distinguished. Furthermore, by removing charged muons using the "01" coincidence (muons comprise 44, 54% in 5 and 25 thick scintillators, and only 5% in the "01" selection), we enlarge the TGE identification power (the observed peak significance). The large-scale electric field that accelerates electrons will decelerate positive muons and accelerate negative muons. However, because the flux of positive muons is higher than the negative, the overall count rate of muons will decrease. Thus, the 25 cm thick SEVAN's scintillator registering gamma rays and muons balanced the deficit of muons and enhancement of TGE gamma rays. In contrast, the "01" coincidence, which eliminates most of the muons by a veto option on charged particles in the upper scintillator, shows a larger enhancement.

To test the new board and to make comparable measurements at Zugspitze and Aragats, we rearranged the CUBE detector on Aragats, previously comprising two spectrometric scintillators surrounded from all sides by six 1 cm. thick scintillators [28]. We modified it to have a similar scintillator configuration to the SEVAN light. The difference is the thickness of the upper veto scintillator and the installation of two spectrometers instead of one (both 20 cm thick). We opted to use a 1 cm thick plastic scintillator because its efficiency in registering gamma rays

Table 1
The share of each of the species of cosmic ray background flux "selected" by different coincidences of the SEVAN light detector.

SEVAN_light Zugspitze	Neutron(%)	Proton(%)	mu+(%)	mu-(%)	e-(%)	e+(%)	Gamma ray(%)
Upper 5cm detector	6.35	7.18	28.5	24.95	12.96	9.98	10.08
Lower 25cm detector	15.84	4.36	22.76	19.83	5.55	4.98	26.69
Coincidence 10	7.27	7.14	26.3	23.08	14.02	10.52	11.67
Coincidence 01	34.25	0.17	2.69	2.45	0.80	0.81	58.80
Coincidence 11	2.84	7.32	36.92	32.1	8.9	7.92	4.01

is very small. Also, it is lightweight, easy to transport, and does not require a large "light-gathering" housing.

Simultaneously with the SEVAN detector, BOLTEK's EFM 100 electric mill [29] was installed at Schneefernerhaus. BOLTEK's electric field sensors are widely used in HEPA research and at large surface arrays measuring EASs [30–32]. Registration of PeV particles by large surface arrays is now accompanied by monitoring atmospheric electric fields. The acceleration and multiplication of EAS electrons in atmospheric electric fields significantly increase the count rates of particle detectors and the surface array trigger frequency, affecting the energy estimates estimated from the shower size [33]. The EFM 100 sensors measuring NSEF with a frequency of 20 Hz estimate the distance to the lightning flash at distances up to 33 km with an accuracy of ≈1.5 km. Last ten years, we have operated networks of ten EFM 100 sensors on the slopes of Mt. Aragats and in Yerevan. Comparisons with the worldwide lightning location network (WWLLN, [34]) show good agreement within the accuracies of both lightning location systems [35]. Using the same type of electric field sensor at sites where SEVAN detectors are installed greatly increases the possibility of multivariate correlation analysis of data from network units. The fast, synchronized data acquisition (FSDAQ [36]) harmonizes signals from particle detectors and electric mills on a nanosecond timescale.

3. TGEs observed by SEVAN light on Zugspitze and CUBE on Aragats on May 23, 2023

On the morning of May 23, during a thunderstorm at Zugspitze, the SEVAN light detector registered sizeable TGE in gamma-ray flux, see Fig.1. At the maximum TGE flux, the enhancement of count rate reached 44% (relative to the count rate measured in fair weather), and the count rate maximum minute intensity significance was 44σ. TGE started at 6:58 when NSEF was in the positive domain +8 kV/m. Then, after briefly touching the negative domain, NSEF returned to the same positive value and was abruptly terminated at 7:06 by a lightning flash that occurred at about 10 km.

Fig. 2 shows the 1-minute time series of count rates measured by the SEVAN light detector's 5 and 25-cm thick scintillators and coincidences selecting charged and neutral particles. The fair-weather flux and the enhancement absolute and relative values at the minute of the maximum TGE flux are shown in the second-fourth columns of the inset in Fig. 2. We present the number of standard deviations above the mean value of fluxes as the significance of the peak in the time series, in the fourth column. The count rate enhancement reaches 44% for the coincidence "01" (green curve) and 25% for the 25 cm scintillator (blue curve). Thus, the "01" coincidence effectively selects TGE gamma rays.

The small enhancement of the 5 cm upper scintillator and "10" coincidence (8 and 9%, black and red curves) evidenced that TGE electrons do not reach the Earth's surface or reach in negligible amounts due to ionization losses in the dense air. In contrast, gamma rays lose only a few tens of percent of the intensity and demonstrate large peaks.

During the night of May 23, a very large TGE occurred on Aragats (Fig. 3). The TGE pattern was similar to that of Zugspitze. The TGE began at 00:16 and finished at 00:35. Normal polarity lightning flashes at 00:34:57 interrupted its progression and abruptly terminated count rate enhancement. The NSEF was mainly in the negative domain. Sometimes, it touched the positive domain before lightning flashed.

Fig. 4 shows the 1-minute time series of count rates measured by 1 and 20-cm thick scintillators of the CUBE detector and the "01"
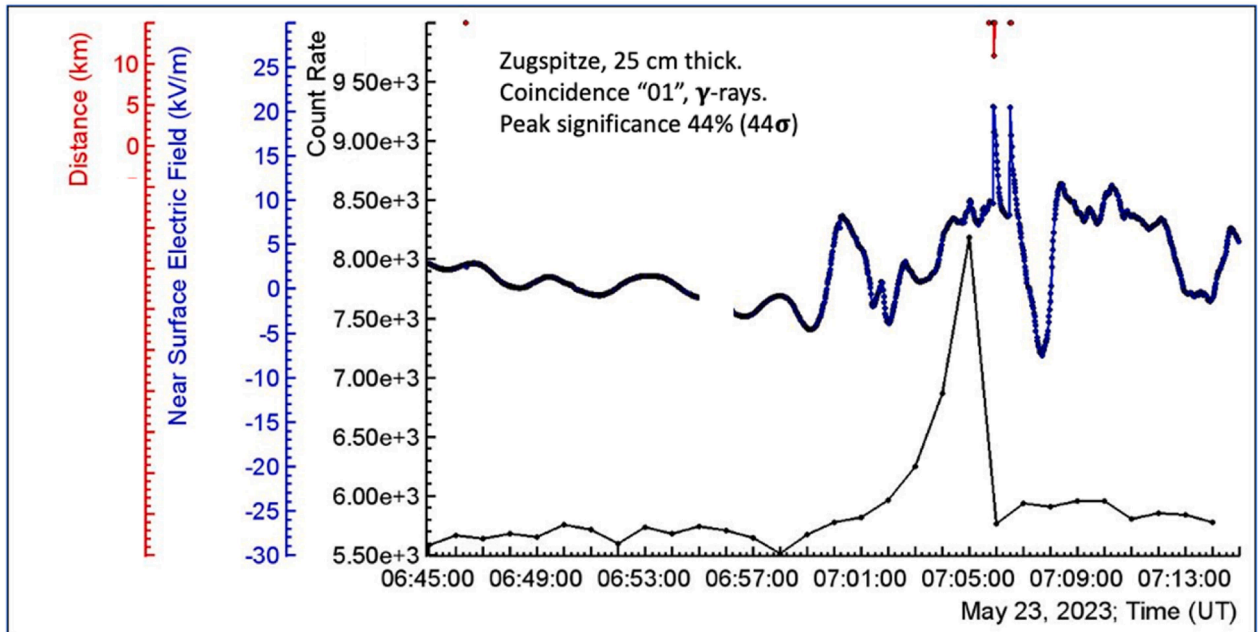

Fig. 1. One minute time series of the "01" coincidence measured by SEVAN light on Zugspitze, black; one second time series of NSEF, blue, and distances to lightning flash, red.
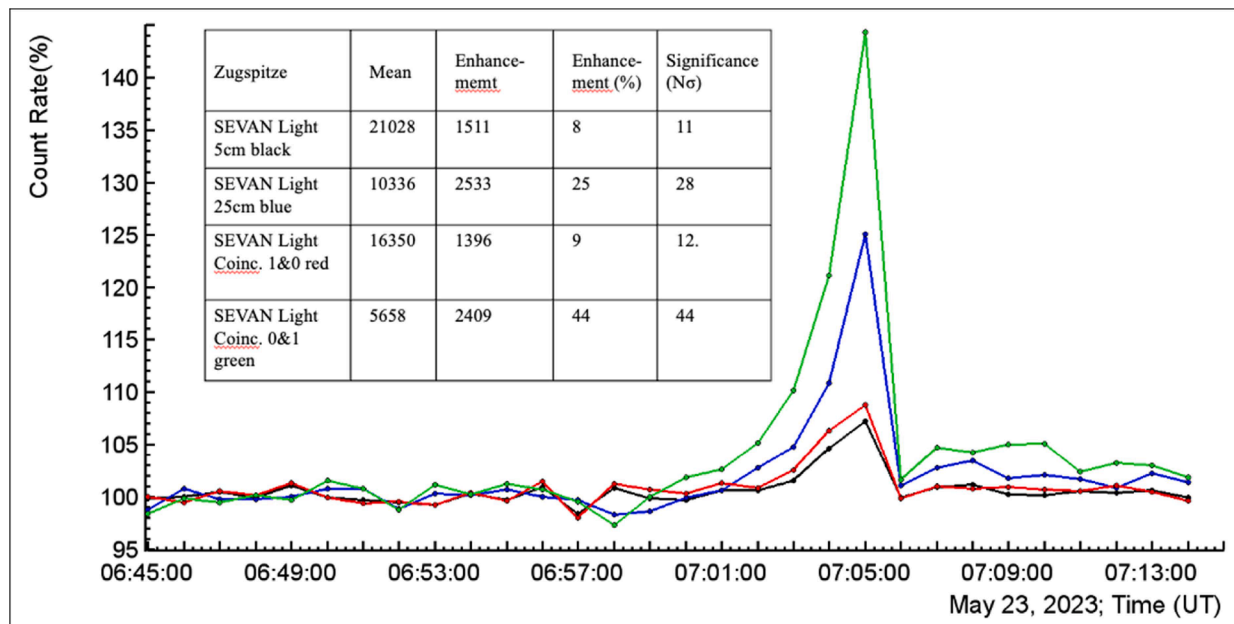
Fig. 2. Time series of TGE showing count rate enhancement relative to fair weather values. In the second column of the inset are shown the mean count rates of 5 and 25-cm thick scintillators of SEVAN light detector at Zugspitze; in the third and fourth columns – absolute and relative values of the count rate enhancement at maximum flux minute. In the last column – the maximum flux significance.
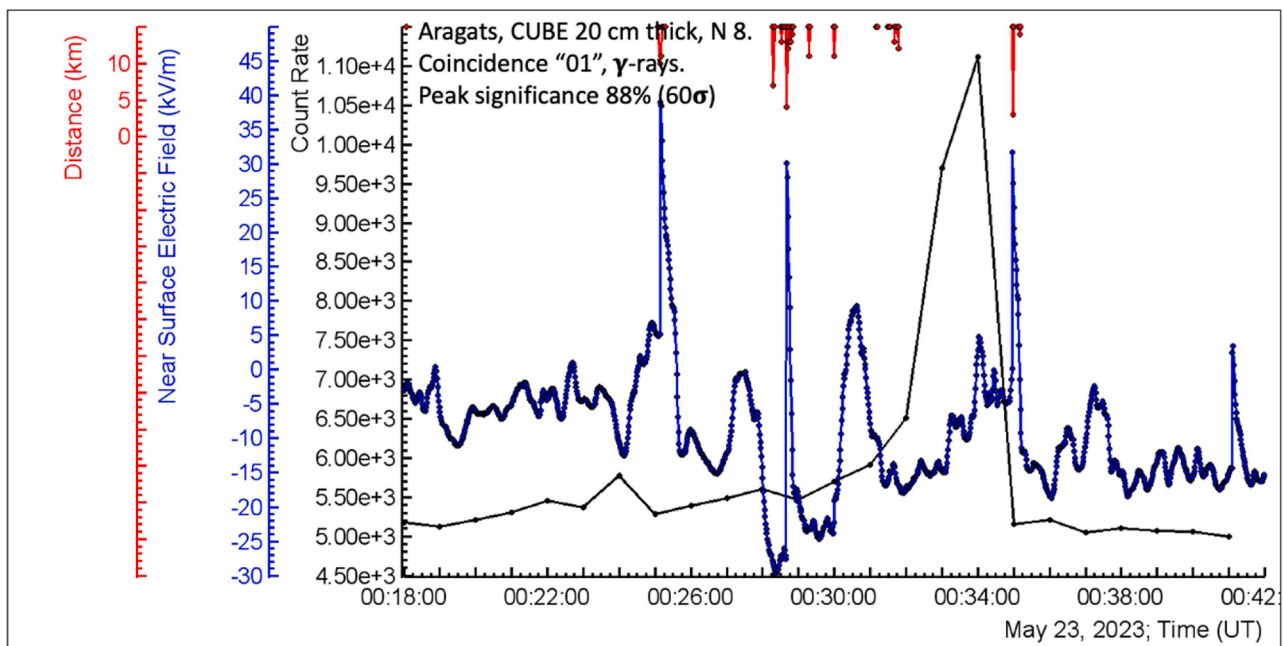

Fig. 3. One minute time series of the "01" coincidence measured by CUBE detector on Aragats, black; One second time series of NSEF, blue, and distances to lightning flash, red.

coincidence selecting neutral particles. The count rate enhancement, shown in Fig. 4, reaches 88% for the coincidence "01" (red curve) and 60% for the 25 cm scintillator (blue curve), much larger than at Zugspitze.

A large enhancement of the 1 cm upper scintillator (88%, black curve) evidenced the enormous flux of TGE electrons at low energies.

Table 2 compares the characteristics of TGEs registered on Aragats and at Zugspiutze.

TGE observed on Aragats occurred during negative NSEF, and TGE at Zugspitze – at positive NSEF. However, they exhibit similar shape, duration, and abrupt termination caused by the normal polarity

lightning flashes. The initial phase of the TGE observed on Aragats lasted longer due to earlier disturbances of the NSEF originating the Radon progeny radiation by the Radon circulation effect [37]. The number of lightning flashes observed during TGEs is posted in the last column of Table 2. On Aragats, in the early stage of TGE development (0:30-0:31:45), 16 lightning flashes were observed within 11-15 km from detectors. No flashes were detected at abrupt rising and a prolonged maximum of TGE after a nearby (2.6 km) flash. Which stopped the TGE; there were 12 flashes within 15 km in 13 seconds. At Zugspitze, there were no flashes before terminating lighting, and after it, eight flashes at distances 11-15 km were observed.
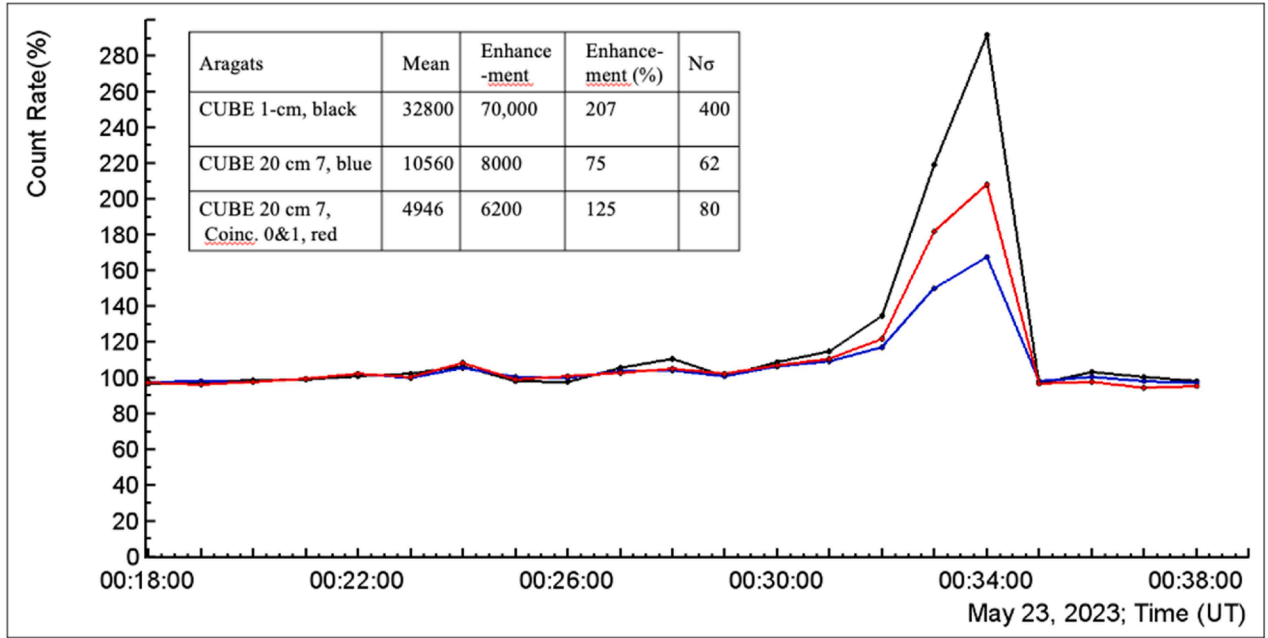
Fig. 4. TGE time series showing count rate enhancement relative to fair weather values on Aragats. The mean count rates of 5 and 20-cm thick scintillators and their coincidences are shown in the second column of the inset. In the third and fourth columns – absolute and relative values of the count rate enhancement at maximum flux minute. In the last column – is the maximum flux significance.

Table 2
Comparison of TGEs observed on Aragats and Zugspitze on May 23, 2023 (peak significance and NSEF).

Time on 23 May 2023	Enhancement %	Nσ	NSEF kV/m	Terminating Lightning and distance	Number of lightning flashes within 15 km
Aragats CUBE 01 coincidence, 0:30 - 0:35	88	60	-18 - -5	00:34:57, 2.6 km	28 flashes at 0:30 – 0:35:10
Zugspitze SEVAN 01 coincidence, 7:01 – 7:06	44	44	0 - +10	7:05:54, 10 km	8 flashes at 7:00 – 7:06

4. TGE electron and gamma-ray energy spectra recovery

In this section, we explain the procedure of recovering energy spectra from energy release histograms and present electron and gamma-ray energy spectra from Aragats and gamma-ray energy spectra from Zugspitze. The Aragats station's CUBE and UFS's SEVAN light detectors electronics continuously recorded 1-minute histograms of particle energy releases. These histograms show the number of events versus the energy released in the detector. Spectrometers used in HEPA physics typically recover spectra up to 10 MeV. However, the Logarithmic Amplitude-Digit Converter (LADC), used in CUBE and SEVAN electronics, has a unique feature that allows to obtain spectra up to 50 MeV [38]. LADC applies a logarithmic function to the input signal. This means that the quantization step size varies depending on the amplitude of the input signal. The LADC can handle a wide dynamic range of input signal amplitudes, compressing higher and expanding lower ones.

The observed energy release distributions differ from the original energy spectrum above detectors due to detector response, which modifies the "genuine" energy to a measured one. Inverse problem solving involves deducing the original energy spectrum of the cosmic rays from the observed energy-release histograms. This is a complex task because the process of cosmic ray interaction and detection distorts the original energy distribution. Estimation of the response function of a detector is a crucial task in energy spectra recovery. It typically involves predicting the outcomes of a known set of inputs (direct problem solving). This contrasts the inverse problem, which aims to determine the unknown causes that lead to observed effects. The response function describes how a detector responds to different particle fluxes with varying energies, i.e., what is the probability of measuring energy deposit E_{dep} if the true energy of a particle is E_{true}. To obtain the response function of a specific detector, we need to solve the direct problem of cosmic rays by starting from known particle fluxes. Particle fluxes at any geographical coordinates and attitudes were obtained from the EXPACS WEB calculator [38]. The CERN GEANT 4 code [39] was used to transport particles via arbitrary media, considering various sources of randomness and uncertainty in the measurement process. Thus, the response matrix will account for the smearing effects due to the finite resolution of the detector and the asymmetry in the bin-to-bin migration due to very steep cosmic ray spectra. The energy release in the detector simulated with GEANT4 was converted to LADC codes with the following expression:

$$[k] = d \cdot \ln\left(E_{dep}/E_0\right) + k_0 \tag{1}$$

Where $[k] \geq 1$ is the LADC code, $d \approx 10.5$ is the LADC scale factor, E_{dep} is the energy release in the plastic scintillator, E_0 is the average muon energy release in the plastic scintillator, and k_0 is the LADC code corresponding to the minimum ionization particle (MIP) loses in the detector.

As a result of simulation trials, we obtain the response matrix, $A_{i,j}$, which shows how the particles with input energy x_j ($j=1, N$) are distributed among measurements y_i (number of events fall in the energy bin i). Thus, the response matrix, $A_{i,j}$, shows the likelihood that an event with actual energy from bin j is measured with energy corresponding to bin i.

$$y_j = A_{i,j} \ x_i \qquad i, j = 1, ..., N \tag{2}$$

The energy deposit E_{dep} (MeV) was simulated for a given set of

energies E_j ($j= 1, N$) covering an energy range from 1 to 100 MeV. The number of energy bins N should be chosen accurately enough to represent all measured energies while avoiding excessive computational burden; we choose N=127. Conversion of energy to LADC codes was done according to eq. (2), M= 100000 events were simulated for each E_j. The response matrix was normalized by the total number of simulation trials, which equals M*N. During the matrix calculation, we considered the particle registration efficiency, which varies depending on the particle's energy. To determine the actual energy spectrum from the measured energy release histogram, we used the unfolding procedure, which involved inverting the response matrix A, to finally obtain the energy spectrum:

$$x_i = A_{i,j}^{-1} y_j \quad i,j = 1, ..., N \tag{3}$$

The derived energy spectra are validated using different detectors and observational methods. The count rates of the SEVAN detector were estimated using the recovered energy spectrum of a large TGE that occurred on 6 October 2021. The experimentally observed and simulated particle fluxes at the maximum of the TGE development showed an agreement of approximately 20% (see Table 2 of [40]).

The TGE spectra were recovered by various spectrometers, including a large 4 m^2 area and 60 cm thick ASNT scintillation spectrometer [41], large ($12 \times 12 \times 30$ cm) NaI (Tl) spectrometers [42], and CUBE scintillation spectrometers. In Fig. 12 of [43], 3 recovered differential energy spectra of a large TGE were compared, and all three spectra coincide rather well. The obtained differential energy spectra of gamma rays and electrons were approximated using a single power function or a five-parameter fit, including spectral knee [44].

In Fig. 5a, we show the histogram of energy releases of particles selected by "01" coincidence in the CUBE detector. This coincidence picks gamma rays because the probability of a signal in the upper 1-cm thick scintillator is very low for gamma rays and very high for electrons. The lower 20-cm thick scintillator is much more efficient in registering gamma rays. Although atmospheric neutrons can also be detected, the flux of neutrons resulting from the photonuclear reactions of TGE gamma-rays is only 1-2% of the TGE gamma-ray flux. Fig. 5b shows the recovered differential energy spectrum of TGE gamma rays. The energy levels below 10 MeV indicate the presence of gamma radiation contamination from Radon progeny. After 10 MeV spectrum becomes steeper, and after 40 MeV, we see the spectrum rise due to the influence of MOS gamma rays [19]. The MOS process adds a small percentage to TGE gamma-ray flux (due to enhanced bremsstrahlung of high energy electrons gaining energy from electric field), not seen at lower energies.

As the TGE flux decreases, the influence of the MOS gamma rays becomes more visible.

Fig. 6 shows the energy release histogram of TGE electrons and the recovered energy spectrum. We refer to relativistic positrons and electrons as electrons for brevity. We use an indirect method to retrieve the electron spectrum. We subtract the energy release histogram "01" (gamma rays) from the energy release histogram in the 20 cm thick scintillator (gamma rays and electrons). The number of gamma rays is much greater at low energies than that of electrons, as shown in Figs. 5a and 6a. Electron flux attenuates significantly faster than that of gamma rays. However, at high energies, the electron and gamma-ray fluxes are close.

Recovering the energy spectrum of electrons is challenging due to the overwhelming flux of gamma rays that typically mask the weak electron flux. However, in the Mendeley dataset [45], we recovered the electron differential energy spectra by analyzing 16 TGE events and estimated the heights of the termination of the field above the ground. The distance at which the strong accelerating field is terminated (free passage distance, FPD) is determined by an empirical equation. The parameters of the equation were fitted by simulations [46].

$$FPL(meters) = \left(C1 * E_{max}^g - E_{max}^e\right)/C2 \tag{4}$$

We read out the highest energies of electrons and gamma rays from recovered energy spectra. Coefficients C1 and C2 are 1.2 and 0.2 consequently. TGE simulations suggest that the maximum energy of electrons going out of the electric field is approximately 20% higher than that of gamma rays. Therefore, we can estimate the maximum energy of electrons leaving the field by C1*E^γ max. Furthermore, we assume that the maximum energy of gamma rays does not change significantly when they travel 100 m or less in the atmosphere. Also, we assume that electrons lose approximately 0.2 MeV per m at altitudes of about 3000m. We conducted multiple simulations of electron-gamma ray avalanches to verify the accuracy of equation (4) to detect any potential methodological errors. We store the particle energies and solve the inverse problem to recover the RREA characteristics from the measured TGE. We utilize CORSIKA simulations with varying electric field strengths and termination heights to achieve this. Subsequently, we apply all experimental procedures to the obtained samples to estimate the maximum energies of electrons and gamma rays. Then, we calculated the FPL parameter by equation (4) and compared it to the "true" value in the simulation. Based on this comparison, we estimate the method's mean square deviation (MSD) to be 50 meters, see Table 12 of [47]. Using the maximum energies of gamma rays (about 50 MeV) and
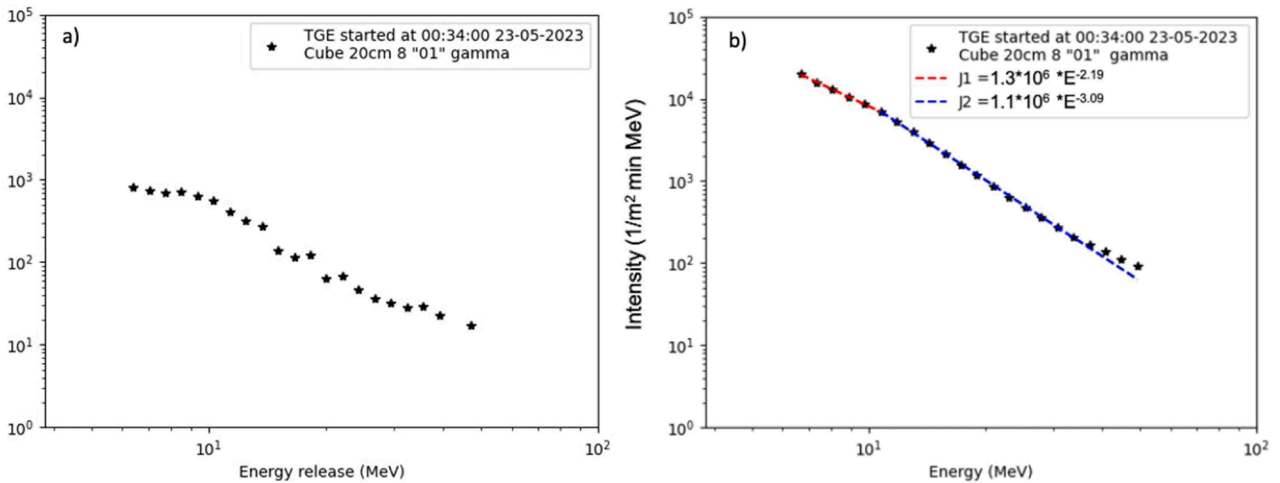

Fig. 5. a) Energy release histogram of particles selected by the "01" coincidence (mainly gamma rays) in the 20-cm thick scintillator of CUBE detector on Aragats; b) differential energy spectrum of TGE gamma rays recovered from energy release histogram using detector response function. In legends, we show parameters of power law fits.
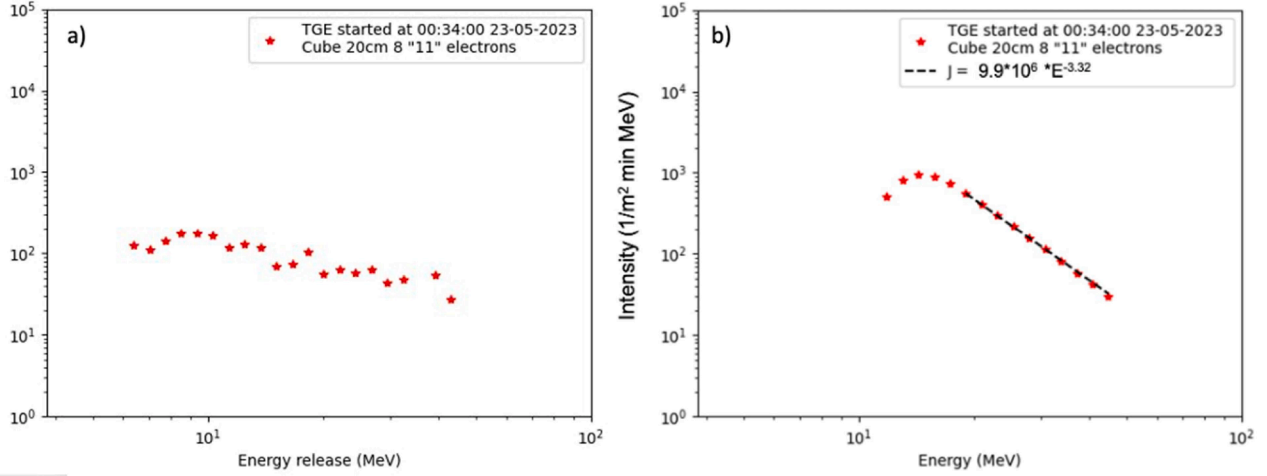
Fig. 6. a) Energy release histogram of particles selected by the subtracting energy release histogram of gamma rays from the total energy release histogram in the 20 cm thick scintillator on Aragats; b) differential energy spectrum of TGE electrons recovered from energy release histogram using detector response function. In legends, we show parameters of power law fit.

electrons (about 45 MeV), see Figs. 5b and 6b, we can estimate H to be 75+/- 50 meters. This estimate may be related to the height of the cloud base. Estimating the height where the strong electric field weakens, we conclude that its strength should be not less than 2.1 kV/m at 75-100 meters above the ground. At 3300 meters, the lower electric field strength is insufficient to impart acceleration to electrons.

In Fig 7a, we show the measured histogram of energy releases of particles selected by "01" coincidence by the SEVAN light detector at Zugspitze. Zugspitze TGE's intensity is lower than Aragats TGE's (Compare Figs 5b and 7b). However, the maximum energy of 60 MeV is larger due to the thickness of the scintillator (25 cm vs. 20 cm of the CUBE detector). The height of the electric field termination was higher than at Aragats; only a few tens of low-energy electrons were registered, and recovery of the electron energy spectrum was not feasible.

5. The atmospheric conditions supporting TGE initiation

This section summarizes the atmospheric conditions measured during TGEs and discusses their possible influence on TGE initiation. Also, we discuss the values of recovered energy spectra. We recover the cloud base height by calculating the spread between the air temperature and dew point according to the well-known approximate equation [48].

$$H(m) \approx (\text{Air temperature } \{°C\} - \text{dew point } \{°C\}) \times 122 \tag{5}$$

Fig. 8 shows the 1-minute time series of outside temperature, solar radiation, and count rate ("01" coincidence of CUBE detector) measured on Aragats. The maximum of the TGE occurred at 00:34, when the outside temperature was 0.3C, 12 minutes before the daily minimum of -0.3C. The calculated cloud base at 0:34 was 30 m. Thus, the cloud base was very close to the Earth's surface during TGE, and fast ions from possible corona discharges can enhance the charge of LPCR, enlarging the potential drop in the lower dipole [49]. The preferred nocturnal occurrence of large TGEs noticed in [49] can reflect this interesting mechanism of atmospheric electric field intensification and TGE flux rise. However, understanding the weather conditions supporting TGE origination is far from fully understood. Positioning the electric field sensors on UAVs above Aragats, now under discussion, will provide valuable information on the dynamics and nature of the atmospheric electric field in the lower atmosphere.

Table 3 compares atmospheric conditions at Zugspitze and on Aragats and gamma-ray energy spectra indices. The weather data are obtained from the DAVIS weather station on Aragats [50] and from the German Meteorological Service (DWD) at UFS [51]. The height where the accelerating atmospheric electric field was terminated (free passage
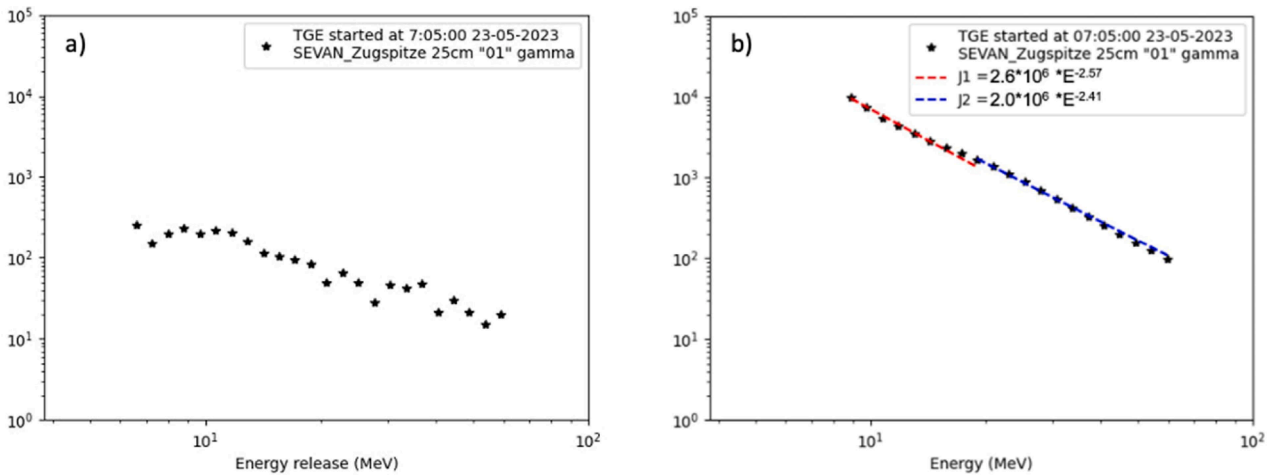

Fig. 7. a) Energy release histogram of particles selected by the "01" coincidence (mainly gamma rays) in the 25 cm scintillator of thick SEVAN light detector at Zugspitze; b) differential energy spectrum of TGE gamma rays recovered from energy release histogram using detector response function. In legends, we show parameters of power law fit.
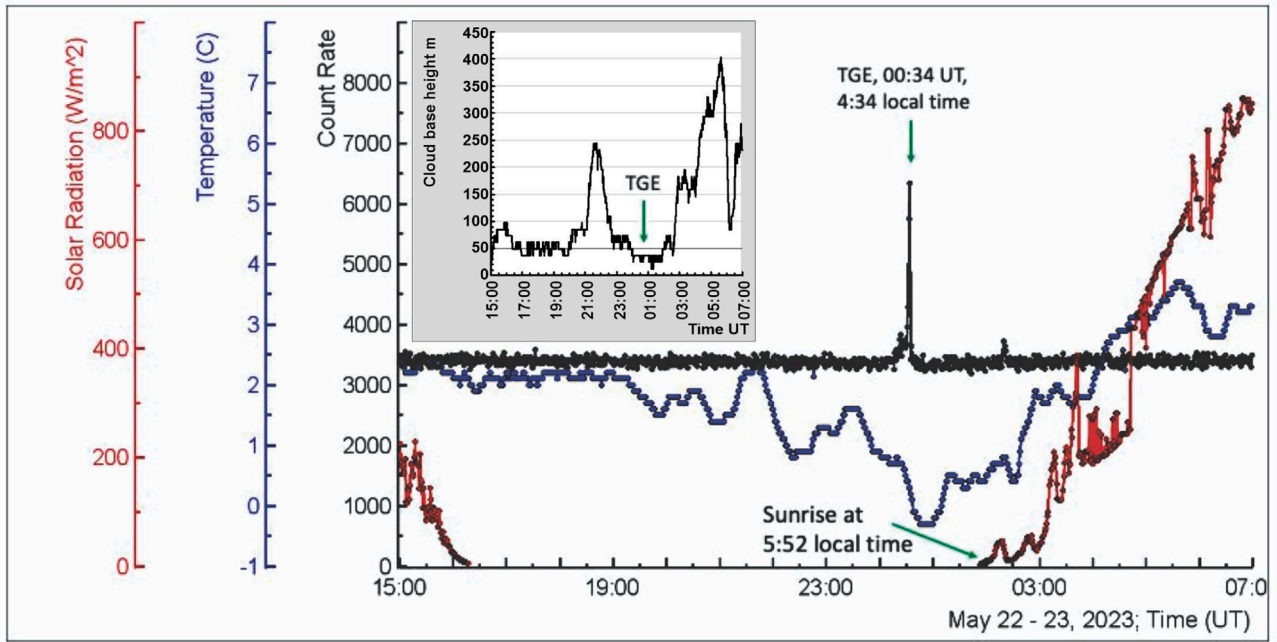
Fig. 8. One-minute time series of the Aragats TGE count rate (CUBE "01" coincidence, black), Outside temperature (blue), and solar radiation (red). In the inset, we show the distance to the cloud base calculated by spread. By green arrows, we show the TGE flux maximum and sunrise.

Table 3
Comparison of TGEs observed on Aragats and Zugspitze on May 23, 2023 (energy spectra and cloud height).

Time on 23 May 2023	Temp. C°	RH %	Cloud Height by equation 5 (m)	FPD by equation 4 (m)	Index of gamma-ray energy spectrum	Index of the electron energy spectrum
Aragats CUBE 01 coincidence 0:30 - 0:35	0.3	98	30	75±50	-3.09	-3.32
Zugspitze SEVAN 01 coincidence 7:01 – 7:06	4.2	96	50	-	-2.38	-

distance) was calculated according to equation 4.

At Zugspitze, TGE occurred in the early morning and exhibited a positive NSEF. It emphasizes the diversity of atmospheric conditions supporting TGE. Each geographical location has its conditions on NSEF, allowing the unleashing of TGE. At Aragats, there is a nearby lake; at Lomnicky Stit, there is a very sharp peak. We need additional TGEs measured at Zugspitze to address this interesting problem. The energy spectrum measured at Zugspitze is smoother than the Aragats spectrum because, as usual, spectra of intense TGEs are sharper compared with weaker spectra (see Fig. 15 of [27]). The electron energy spectrum is sharper than the gamma-ray energy spectrum due to the fast decline of electron flux in the dense atmosphere.

6. Conclusions

SEVAN detectors offer new possibilities for measuring energy spectra of gamma rays and electrons during thunderstorms and neutrons during violent solar flares. These options are unique for studying high-energy atmospheric physics and solar physics. Until now, the TGE electron energy spectra were only measured on Aragats Mountain. Detectors located on mountain altitudes, just under particle avalanches developed above, register millions of particles for each TGE event. This allows for reaching high statistical significance of the TGE detection and recovering energy spectra. Additionally, we can estimate the height and strength of the intracloud electric fields from the recovered spectra. The closeness of the time series of count rates and recovered energy spectra

evident from TGE observation on Mountain peaks in Eastern Europe and Germany support the universality of the physical phenomenon of RREA/ TGE. On May 23, a very large TGE was discovered at Aragats, one of the four largest on record. This TGE allows recovery of gamma-ray and electron energy spectra, demonstrating new possibilities of CUBE and SEVAN light detectors equipped with LADCs. The TGE observed at the Zugspitze was smaller, and few electrons reached the 25 cm thick spectrometric scintillator. The electron flux was attenuated in the dense air, the body of the 5 cm thick scintillator, and its iron housing.

Studying TGEs is complex and challenging due to thunderstorms' dynamic and chaotic nature of the atmospheric electric field. However, the newly installed research facilities on the Aragats and Zugspitze mountains will be vital in understanding the intricate relationship between particle fluxes, electric fields, and weather conditions. These facilities will provide valuable insights into the research of TGEs. In conclusion, the new possibilities offered by SEVAN detectors give a unique opportunity for high-energy atmospheric physics and solar physics research. The recovered spectra, coupled with the ability to estimate the height and strength of intracloud electric fields, significantly advance high-energy atmospheric physics research.

CRediT authorship contribution statement

A. Chilingarian: Writing – review & editing, Writing – original draft, Visualization, Supervision, Methodology, Investigation, Funding acquisition, Formal analysis, Conceptualization. **T. Karapetyan:** Resources,

Methodology, Investigation. **B. Sargsyan:** Visualization, Validation, Software, Methodology, Investigation, Formal analysis. **J. Knapp:** Funding acquisition, Formal analysis, Data curation. **M. Walter:** Methodology, Funding acquisition, Data curation. **T. Rehm:** Resources, Funding acquisition, Formal analysis, Data curation.

Declaration of competing interest

The authors declare that they have no known competing financial interests or personal relationships that could have appeared to influence the work reported in this paper.

Data availability

Data will be made available on request.

Acknowledgments

References

[1] A. Chilingarian, G. Hovsepyan, K. Arakelyan, S. Chilingaryan, V. Danielyan, K. Avakyan, et al., Space environmental viewing and analysis network (SEVAN), Earth Moon Planets 104 (2009) 195.

[2] A. Chilingarian, A. Reymers, Particle detectors in Solar Physics and Space Weather Research, Astropart. Phys. 27 (2007) 465–472.

[3] N. Gevorgyan, V. Babayan, A. Chilingarian, H. Martirosyan, Test alert service against very large SEP Events, Advances in Space Research 36 (2005) 2351–2356.

[4] A. Chilingarian, V. Babayan, T. Karapetyan, et al., The SEVAN Worldwide network of particle detectors: 10 years of operation, Advances in Space Research 61 (2018) 2680–2696.

[5] J.R. Dwyer, D.M. Smith, S.A. Cummer, High-Energy Atmospheric Physics: Terrestrial Gamma-Ray Flashes and Related Phenomena, Space Science Review 173 (2012) 133.

[6] A. Chilingarian, A. Daryan, K. Arakelyan, et al., Ground-based observations of thunderstorm-correlated fluxes of high-energy electrons, gamma rays, and neutrons, Phys. Rev. D 82 (2010) 043009.

[7] A. Chilingarian, G. Hovsepyan, A. Hovhannisyan, Particle bursts from thunderclouds: Natural particle accelerators above our heads, Phys. Rev. D 83 (2011) 062001.

[8] G.J. Fishman, P.N. Bhat, R. Mallozzi, et al., Discovery of Intense Gamma-Ray Flashes of Atmospheric Origin, Science 264 (1994) 1313.

[9] M. McCarthy, G. Parks, Further observations of X-rays inside thunderstorms, Geophysical Research Letters 12 (1985) 393.

[10] H. Tsuchiya, T. Enoto, S. Yamada, et al., Detection of high-energy gamma rays from winter thunderclouds, Phys. Rev. Lett. 99 (2007) 165002.

[11] N.A. Kelley, D.M. Smith, J.R. Dwyer, et al., Relativistic electron avalanches as a thunderstorm discharge competing with lightning, Nature Communications 6 (2015).

[12] P. Auger, et al., Extensive Cosmic-Ray Showers, Reviews of Modern Physics 11 (3–4) (1939) 288–291.

[13] A.V. Gurevich, G.M. Milikh, R.A. Roussel-Dupre, Runaway electron mechanism of air breakdown and preconditioning during a thunderstorm, Phys. Lett. 165A (1992) 463.

[14] J.R. Dwyer, Relativistic breakdown in planetary atmospheres, Physics of Plasmas 14 (2007) 042901.

[15] L.P. Babich, E.N. Donskoy, I.M. Kutsyk, et al., IEEE Trans. Plasma Sci 29 (3) (2001) 430.

[16] VV Alexeenko, NS Khaerdinov, AS Lidvansky, et al., Transient variations of secondary cosmic rays due to atmospheric electric field and evidence for pre-lightning particle acceleration, Phys Lett A 301 (2002) 299–306.

[17] J.R. Dwyer, A fundamental limit on electric fields in air, Geophys. Res. Lett. 30 (2003) 2055.

[18] L.I. Dorman, I.V. Dorman, Possible influence of cosmic rays on climate through thunderstorm clouds, Adv. Space Res. 35 (2005) 476.

[19] A. Chilingarian, B. Mailyan, L. Vanyan, Recovering the energy spectra of electrons and gamma rays coming from the thunderclouds, Atmos. Res. 114–115 (2012) 1.

[20] A. Chilingarian, T. Karapetyan, M. Zazyan, G. Hovsepyan, B. Sargsyan, N. Nikolova, H. Angelov, J. Chum, R. Langer, Maximum strength of the atmospheric electric field, Phys. Rev. D 103 (2021) 043021.

[21] A. Chilingarian, G. Hovsepyan, Y. Khanikyanc, A. Reymers, S. Soghomonyan, Lightning origination and thunderstorm ground enhancements terminated by the lightning flash, EPL 110 (2015) 49001.

[22] A. Chilingarian, Y. Khanikyants, E. Mareev, D. Pokhsraryan, V.A. Rakov, S. Soghomonyan, Types of lightning discharges that abruptly terminate enhanced fluxes of energetic radiation and particles observed at ground level, J. Geophys. Res. Atmos. 122 (2017) 7582–7599.

[23] A. Chilingarian, G. Hovsepyan, D. Aslanyan, T. Karapetyan, Y. Khanikyanc, B. Sargsyan L.Kozliner, S. Soghomonyan, S. Chilingaryan, D. Pokhsraryan, M. Zazyan, Thunderstorm Ground Enhancements: Multivariate analysis of 12 years of observations, Physical Review D 106 (2022) 082004, 2022.

[24] Y. Wada T. Matsumoto, T. Enoto, et al., Catalog of gamma-ray glow during four winter seasons in Japan, Physical Review Research 3 (2021) 043117.

[25] J. Kuettner, The electrical and meteorological conditions inside thunderclouds, J. Meteorol. 7 (1950) 322.

[26] Mares, V., Brall, T., Bütikofer, R., Rühm, W., (2020), Influence of environmental parameters on secondary cosmic ray neutrons at high-altitude research stations at Jungfraujoch, Switzerland, and Zugspitze, Germany, Radiation Physics and Chemistry, 168, 10.1016/j.radphyschem.2019.108557.

[27] Sato, Analytical model for estimating the zenith angle dependence of terrestrial cosmic ray fluxes, PLOS ONE 11 (2016) e0160390.

[28] A. Chilingarian, G. Hovsepyan, L. Kozliner, Thunderstorm ground enhancements: Gamma-ray differential energy spectra, Physical Review D 88 (2013) 073001.

[29] Available online: https://www.boltek.com/EFM-100C_Manual_030323.pdf (accessed on 1 January 2024).

[30] B.Bartoli Axikegu, P. Bernardini, et al., Cosmic ray shower rate variations detected by the ARGO-YBJ experiment during thunderstorms, PHYSICAL REVIEW D 106 (2022) 022008.

[31] F. Aharonian, An Q Axikegu, et al., Flux Variations of Cosmic Ray Air Showers Detected by LHAASO-KM2A During a Thunderstorm on 10, Chinese Physics C 47 (June 2021) 015001, 2022.

[32] A.U. Abeysekara, J.A. Aguilar, S. Aguilar, et al., On the sensitivity of the HAWC observatory to gamma-ray bursts, Astropart. Phys. 35 (2012) 641, https://doi.org/10.1016/j.astropartphys.2012.02.001.

[33] A Chilingarian, G Hovsepyan, M Zazyan, Sinergy of extra-terrestrial particle accelerators and accelerators operating in the terrestrial atmosphere, J. Phys.: Conf. Ser. 2398 (2022) 012001.

[34] C.J. Rodger, J. Brundell, R.L. Dowden, Location accuracy of VLF World-Wide Lightning Location (WWLL) network: Post-algorithm upgrade, Ann. Geophys. 23 (2005) 277–290.

[35] Suren Soghomonyan, Ashot Chilingarian, Thunderstorm ground enhancements abruptly terminated by a lightning flash registered both by WWLLN and local network of EFM-100 electric mills. Mendeley Data, 2021, p. V1, https://doi.org/10.17632/ygvjzdx3w3. https://data.mendeley.com/datasets/ygvjzdx3w3/1.

[36] S.Soghomonyan A.Chilingarian, Y. Khanikyanc, D. Pokhsraryan, On the origin of particle fluxes from thunderclouds, Astroparticle Physics 105 (54) (2019).

[37] A. Chilingarian, G. Hovsepyan, B. Sargsyan, Circulation of Radon progeny in the terrestrial atmosphere during thunderstorms, Geophysical Research Letters 47 (2020) e2020GL091155, https://doi.org/10.1029/2020GL091155.

[38] A. Chilingarian, G. Hovsepyan, T. Karapetyan, B. Sarsyan, S. Chilingaryan, Measurements of energy spectra of relativistic electrons and gamma-rays avalanches developed in the thunderous atmosphere with Aragats Solar Neutron Telescope, Journal of Instrumentation 17 (2022) P03002.

[39] GEANT4 collaboration, GEANT4–a simulation toolkit, Nucl. Instrum. Meth. A 506 (2003) 250.

[40] A. Chilingarian, G. Hovsepyan, T. Karapetyan, Y. Khanykyanc, D. Pokhsraryan, B. Sargsyan, S. Chilingaryan, S. Soghomonyan, Multi-messenger observations of thunderstorm-related bursts of cosmic rays, JINST 17 (2022) P07022.

[41] G.Hovsepyan A.Chilingarian, L.Kozliner T.Karapetyan, S.Chilingaryan. D. Pokhsraryan, B. Sargsyan, The horizontal profile of the atmospheric electric fields as measured during thunderstorms by the network of NaI spectrometers located on the slopes of Mt, Aragats 17 (2022) P10011.

[42] A. Chilingarian, S. Chilingaryan, G. Hovsepyan, Calibration of particle detectors for secondary cosmic rays using gamma-ray beams from thunderclouds, Astroparticle Physics 69 (2015) 37–43.

[43] A. Chilingarian, G. Hovsepyan, D. Aslanyan, et al., Thunderstorm ground enhancements observed on Aragats mountain in Armenia in the wintertime, EPL 143, 59002, 10.1209/0295-5075/acf340, supplemented materials.

[44] A. Chilingarian, G. Hovsepyan, T. Karapetyan, D. Aslanyan, S. Chilingaryan, B. Sargsyan, Genesis of thunderstorm ground enhancements, Physical Review D 107 (2023) 102003.

[45] Ashot Chilingarian, Gagik Hovsepyan, "Dataset for 16 parameters of ten thunderstorm ground enhancements (TGEs) allowing recovery of electron energy spectra and estimation the structure of the electric field above earth's surface", Mendeley Data (2021) V3, https://doi.org/10.17632/tvbn6wdf85.3. https://data.mendeley.com/datasets/tvbn6wdf85/3.

[46] G.Hovsepyan A.Chilingarian, M. Zazyan, Measurement of TGE particle energy spectra: An insight in the cloud charge structure, Europhysics Letters 134 (2021) 6901, https://doi.org/10.1209/0295- 5075/ac0dfa.

[47] A. Chilingarian, G. Hovsepyan, D. Aslanyan, et al., Thunderstorm ground enhancements observed on Aragats mountain in Armenia in the wintertime, EPL 143, 59002, Supplemented materials 10.1209/0295-5075/acf340.

[48] Available online, accessed on (1 January 2024). https://www.omnicalculator.com/physics/cloud-base.

[49] E. Williams, B. Mailyan, G. Karapetyan, H. Mkrtchyan, Conditions for energetic electrons and gamma rays in thunderstorm ground enhancements, Journal of Geophysical Research: Atmospheres 128 (2023) e2023JD039612, https://doi.org/10.1029/2023JD039612.

[50] Available online, accessed on (1 January 2024). https://www.davisweatherstation.com/.

[51] Available online, accessed on (1 January 2024). https://schneefernerhaus.de/en/research/members-of-the-consortium/deutscher-wetterdienst/.

[52] Available online, accessed on (1 January 2024). http://adei.crd.yerphi.am/.